


FULL PAPER

Open Access



# A confirmation of vertical acoustic resonance and field-aligned current generation just after the 2022 Hunga Tonga Hunga Ha'apai volcanic eruption

Toshihiko Iyemori<sup>1\*</sup> , Michi Nishioka<sup>2</sup>, Yuichi Otsuka<sup>3</sup> and Atsuki Shinbori<sup>3</sup>

## Abstract

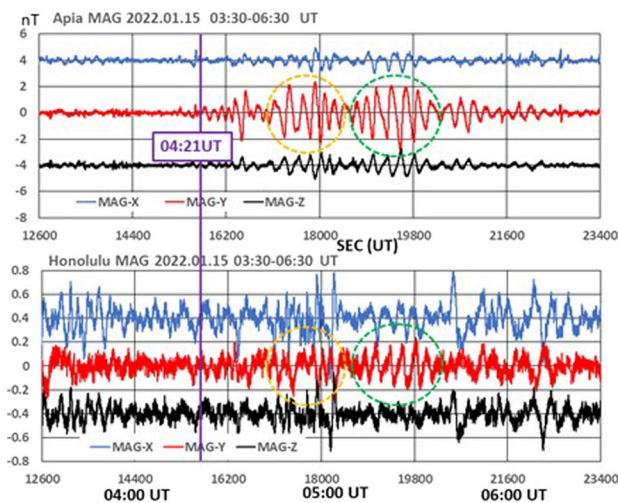
A strong volcanic eruption caused a clear vertical acoustic resonance between the sea surface and the thermosphere. Its effects are observed as geomagnetic and GPS-TEC oscillations near the volcano and its geomagnetic conjugate area. The geomagnetic oscillations are observed at Apia and Honolulu geomagnetic observatories with amplitude of about 2 nT and 0.2 nT, respectively. The volcanic eruption started around 04:14 UT on January 15, 2022. The oscillations appeared at 04:21 UT at Apia, Samoa, only about 7 min after the start of eruption. Because the distance between the volcano and Apia is about 841 km, it takes about 40 min for a sound wave to propagate from the volcano to Apia. Therefore, it is more plausible to assume that the magnetic oscillation observed at Apia about 7 min after the eruption is caused by the sound waves propagated vertically upward to the ionosphere and generated an electric current. The coherent appearance of geomagnetic oscillation at Honolulu located near the geomagnetic conjugate point of the volcano strongly support the idea that the ionospheric current generated over the volcano diverted as a field-aligned current which flew to the opposite hemisphere and caused the geomagnetic oscillation at Honolulu. The earliest start of GPS-TEC oscillation was around 04:15 UT near the volcanic eruption, and it was around 04:20 UT at KOKV station in Hawaii. The time-lag of the TEC variations between Samoa and Hawaii obtained by a cross-correlation analysis is 4.5 min or 8.5 min. These time differences are much smaller than the travel time of the seismic waves from the volcano to Hawaii islands. Therefore, it is suggested that the electric field transmitted along geomagnetic field caused the TEC variation observed over Hawaii Islands. A sawtooth waveform of geomagnetic oscillation observed at Apia and Honolulu is analyzed and a possible generation mechanism is discussed.

**Keywords:** Acoustic resonance, Field-aligned currents, Geomagnetic conjugacy, Geomagnetic field oscillation, GPS-TEC oscillation, Ionospheric current, Volcanic eruption, Sawtooth waveform, Power spectra

\*Correspondence: iyemori.toshihiko.7w@kyoto-u.jp

<sup>1</sup> Graduate School of Science, Kyoto University, Kita-Shirakawa Oiwake-cho, Sakyo-ku, Kyoto 606-8502, Japan  
Full list of author information is available at the end of the article

## Graphical Abstract



## Introduction

The lower atmospheric waves such as acoustic waves or internal gravity waves cause various phenomena in the ionosphere. In some special events such as huge Earthquakes, strong volcanic eruptions, typhoons or tornados, the vertical acoustic resonance between the ground and thermosphere has been observed by various instruments such as seismometer, barometer, magnetometer, GPS, etc. (e.g., Kanamori and Mori 1992; Calais and Minster 1995; Iyemori et al. 2005; Choosakul et al. 2009; Nishioka et al. 2013; Saito et al. 2011). One famous event is the 1991 Pinatubo eruption when the world-wide seismometer network observed a long-period ground oscillation having a resonance period of 3.7 mHz (period of 270 s). Kanamori and Mori (1992) and Kanamori et al. (1994) explained it by the atmospheric pressure variation caused by the resonance. During the 2004 Sumatra Earthquake, a geomagnetic oscillation having another, i.e., first overtone, resonance period of 4.6 mHz (period of 216 s) was observed and it was also explained as the effect of resonance (Iyemori et al. 2005; Shinagawa et al. 2007). The geomagnetic oscillations were explained as a field-aligned current effect caused by the ionospheric dynamo driven by the acoustic waves. A simulation study also confirmed such process (Zettergren and Snively 2015). In the case of Sumatra earthquake, a geomagnetic station at Phimai, Thailand, was near a magnetic conjugate point of the epicenter of Sumatra earthquake. However, there was no geomagnetic station near the epicenter. Therefore, simultaneous and coherent appearance of

geomagnetic oscillation at both geomagnetic conjugate points was not confirmed. During the 2015 eruption of Chile's Calbuco volcano, a satellite observation over the volcanic eruption and the GPS-TEC observation near the volcano suggested the formation of a field-aligned current system caused by the atmospheric waves with acoustic resonance period (Aoyama et al. 2016). In this case, a pair of geomagnetic conjugate observation was also not available.

On January 15, 2022, a submarine volcano, Hunga Tonga Hunga Ha'apai in South Pacific Ocean erupted at around 04:14 UT, and it caused strong atmospheric pressure waves. The pressure pulses were observed worldwide and it caused tsunami in Pacific rim area. During this volcanic eruption event, a geomagnetic observatory, Apia, Samoa, which locates about 841 km north of the volcano observed a short-period oscillation with amplitude about a few nT. Near the geomagnetic conjugate point, a geomagnetic observatory, Honolulu, observed a very small amplitude (less than 0.2 nT) oscillation coherent (but anti-phase) with the oscillation observed at Apia observatory. Near the two geomagnetic stations, GPS receivers were also in operation. If a field-aligned current system is formed, an electric field is also transmitted to the opposite hemisphere along geomagnetic field because the conductance along magnetic lines of force is very high. The transmitted electric field may move the plasmas and could cause electron density fluctuations. Therefore, it is expected that the electron density fluctuations are observed as the GPS-TEC oscillations.

In this paper, we report and discuss the conjugate appearance of geomagnetic and GPS-TEC oscillations and their power spectra.

### Data and method of analysis

The location of the Hunga Tonga Hunga Ha'apai submarine volcano is around (20.546 S, 184.610 E) and, according to the USGS, the eruption started around 04:14:45UT (<https://earthquake.usgs.gov/earthquakes/eventpage/pt22015050/origin/detail>).

One-second resolution geomagnetic data observed at Apia station (13.807 S, 188.225 E) in Samoa and at Honolulu station (21.320 N, 202.000 E) in Hawaii published from the INTERMAGNET web page (<https://intermag-net.org/data-donnee/download-eng.php>) are used in this paper. The coordinate system used in this analysis is XYZ for Apia and HDZ for Honolulu. The geomagnetic conjugate point of the volcano estimated by tracing the IGRF-12 main field model (see <http://www.ngdc.noaa.gov/IAGA/vmod/igrf.html>) from the volcano is at around (25.42 N, 192.99 E).

The GPS-TEC values are derived from 30-s resolution GPS data downloaded from the web sites, UNIVACO and Geoscience Australia. In this paper, we use the SAMO station (13.849 S, 188.262 E) in Samoa, the KOKV

station (22.126 N, 200.335 E) in Kauai Island, and MKEA station (19.801 N, 204.544 E) in Hawaii Island. TEC along the ray path of the radio wave between the GPS satellite and receiver was obtained from the carrier phase and group delays (P-code pseudoranges) of dual-frequency (1.57542 GHz and 1.22760 GHz) GPS signals every 30 s. The ambiguity in the phase measurements due to the unknown initialization constant was corrected by the TEC obtained from the corresponding pseudorange data (Otsuka et al. 2002). The TEC values used in this paper are vertical TEC converted from slant TEC.

The power spectral density (PSD) of the geomagnetic and GPS-TEC data are calculated by the MEM (maximum entropy method). The lag in the MEM calculation is set to be 1/3 of the data length. We also use the FFT (fast Fourier transformation) method when we need to obtain not only PSD, but also phase information. The resolution of period is set to be one second in the MEM calculation even if the temporal resolution of the original GPS data is 30 s.

### Results

Figure 1 shows the geomagnetic data observed at Apia (left panel) and Honolulu (right panel). Note that, for the Honolulu data, the original "D" (declination angle) is

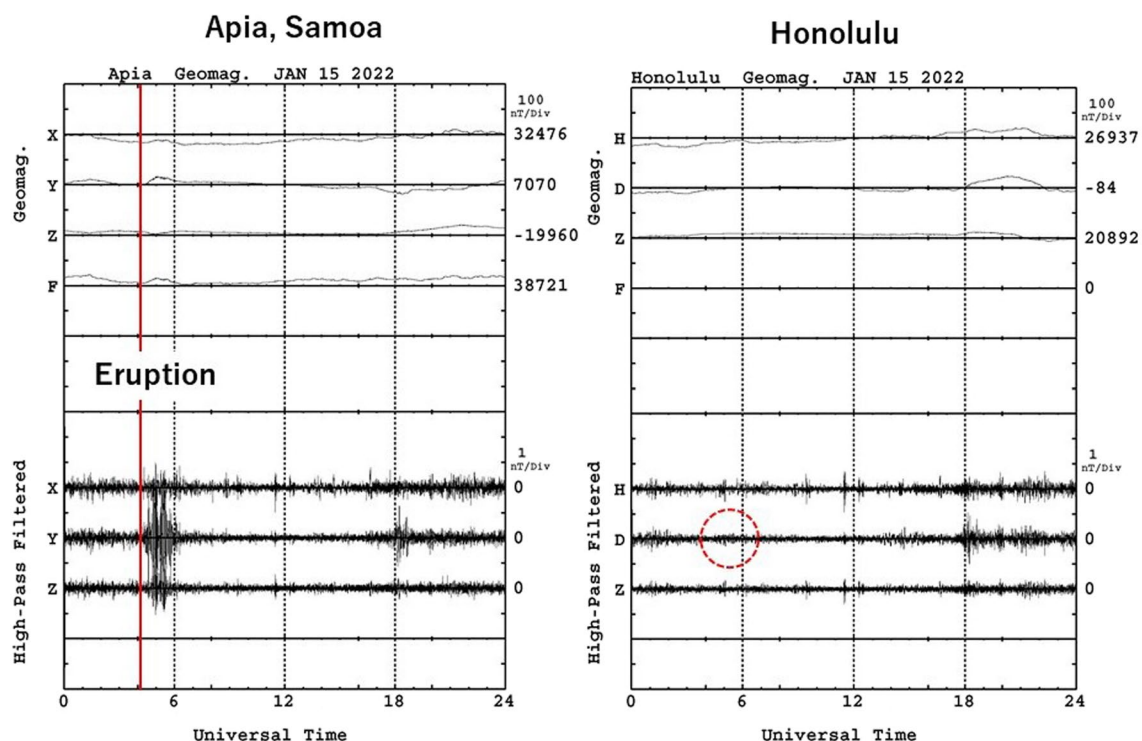


**Fig. 1** Geomagnetic field variation at Apia and Honolulu. The upper 4 traces are the variations after baseline subtraction and the lower 3 traces shows the high-pass filtered data. Note that the D-component of Honolulu data are converted to nT unit in approximately eastward positive

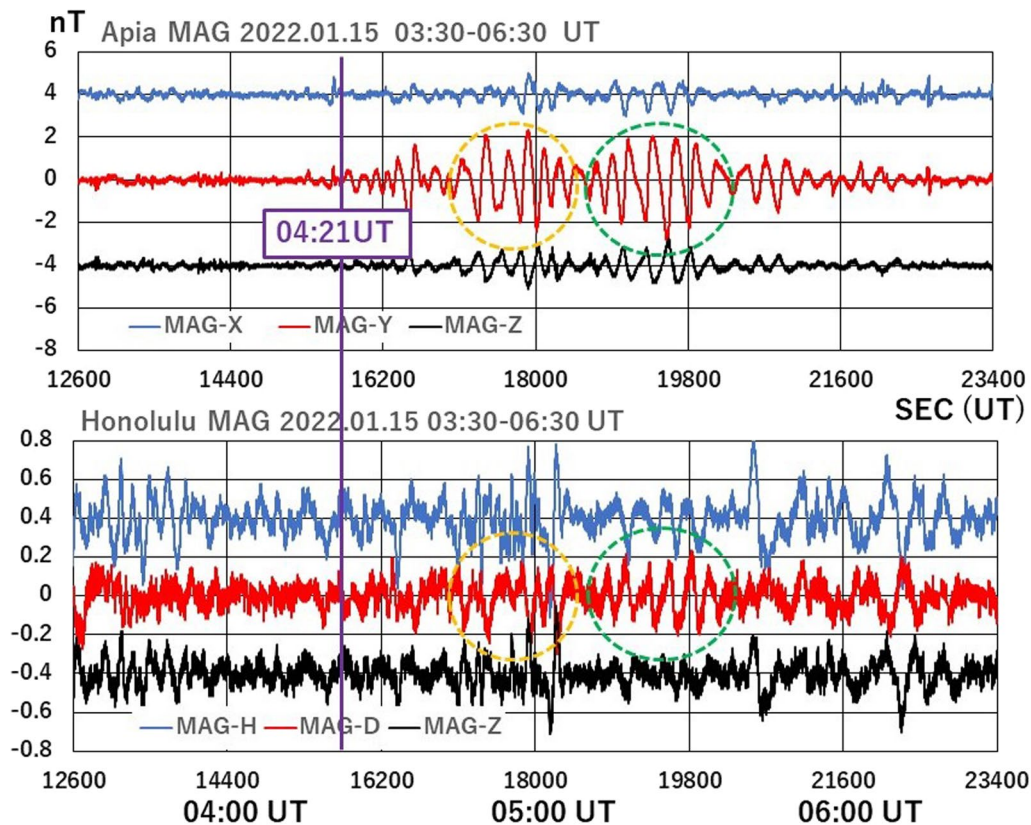


**Fig. 2** Enlarged plots of high-pass filtered geomagnetic components. An oscillation at Apia start around 04:21 UT, about 7 min after the start of eruption. Although the amplitude is small, coherent oscillations with those in Apia encircled by orange and green dotted lines are observed at Honolulu

converted to approximately eastward component (Y) in nT unit, but indicated with symbol “D” in Figs. 1, 2, 7, 8 and 10. The upper 4 traces are observed values with baseline values on the right of each panel. The lower traces are high-pass filtered data by a Gaussian-type weight function with a standard deviation  $\sigma = 120$  s. The cutoff of this filter is around 6 min if we take  $3\sigma$  as a cutoff. However, the cutoff of the Gaussian filter is not very sharp and the variations with period longer than 10 min still remain to some extent.

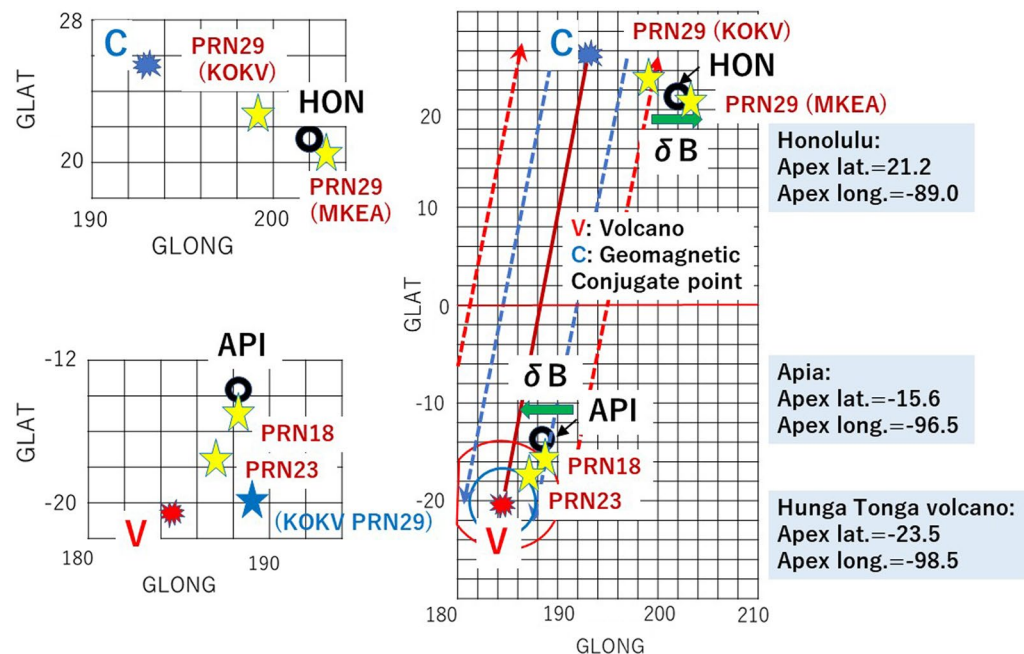
Just after the start of eruption around 04:14 UT, a short-period oscillation with amplitude about a few nT is observed at Apia mainly in eastward component. At Honolulu, a small fluctuation is seen, but it is almost the same amplitude with other periods. However, as shown in Fig. 2, if we expand the time and amplitude scales, we see clearly a coherent oscillation with that at Apia.

Figure 3 illustrates the location of the volcano (indicated by ‘V’) and geomagnetic observatories, and direction of geomagnetic field oscillation at a certain moment. Although Apia and Honolulu are not necessarily very close to the geomagnetic conjugate points each other but

about 500 km apart from conjugate position, it is a distance at which we can expect a common magnetic variation to appear. From the volcano, Honolulu is about  $9^\circ$  apart in geomagnetic longitude. On the other hand, Apia is only  $2^\circ$  apart. This difference may cause the amplitude difference of short-period oscillation, i.e., 2.0 nT for Apia and about 0.2 nT for Honolulu. The ionospheric conductivity may also affect the amplitude difference because Apia was in the summer hemisphere but Honolulu was in the winter hemisphere. The longitudinal difference about  $14^\circ$ , which is nearly 1-h local time, also makes the ionospheric conductivity over Honolulu lower than that over Apia.

To estimate the effect of conductivity difference, the height-integrated ionospheric conductivities integrated in a 100–150 km altitude range,  $\Sigma_p$  (Pedersen) and  $\Sigma_h$  (Hall), are estimated, respectively, to be 8.3 S (siemens) and 12.6 S at 05:00 UT over Apia by using a web service by the World Data Center (WDC) for Geomagnetism, Kyoto. On the other hand, the  $\Sigma_p$  and  $\Sigma_h$  over Honolulu are 1.9 S and 3.2 S, respectively. That is, the conductivities are about 4 times higher in Samoa area than those in





**Fig. 3** Location of the volcano (V), its geomagnetic conjugate point (C), Apia and Honolulu geomagnetic observatories (marked by black circles). Dotted red and blue lines with arrow are schematic presentation of oscillating field-aligned currents and thick green arrows present the direction of magnetic field variation at a certain moment. The blue and red circles present expanding atmospheric waves generated by the eruption. The yellow star marks present the location of the line-of-sight intersection, IPP (ionospheric pierce point) at an altitude of 300 km in the ionosphere to GPS PRN29, PRN23 and PRN18 satellites from the receivers at KOKV (22.126 N, 200.335 E), MKEA (19.801 N, 204.544 E) and SAMO (13.849 S, 188.262 E), respectively. Apex latitudes and longitudes of Apia, Honolulu and the volcano are also presented on the right of the figure. Enlarged maps around Samoa and Hawaii are presented on the left. The blue star symbol indicates the location of geomagnetic conjugate point of the IPP between PRN29 and KOKV at 04:30 UT, (19.8 S, 191.0 E)

Hawaii area. However, this difference, i.e., 4 times, is not enough to explain the observed amplitude difference, i.e., about 10 times. The geomagnetic longitudinal difference may also cause the amplitude difference.

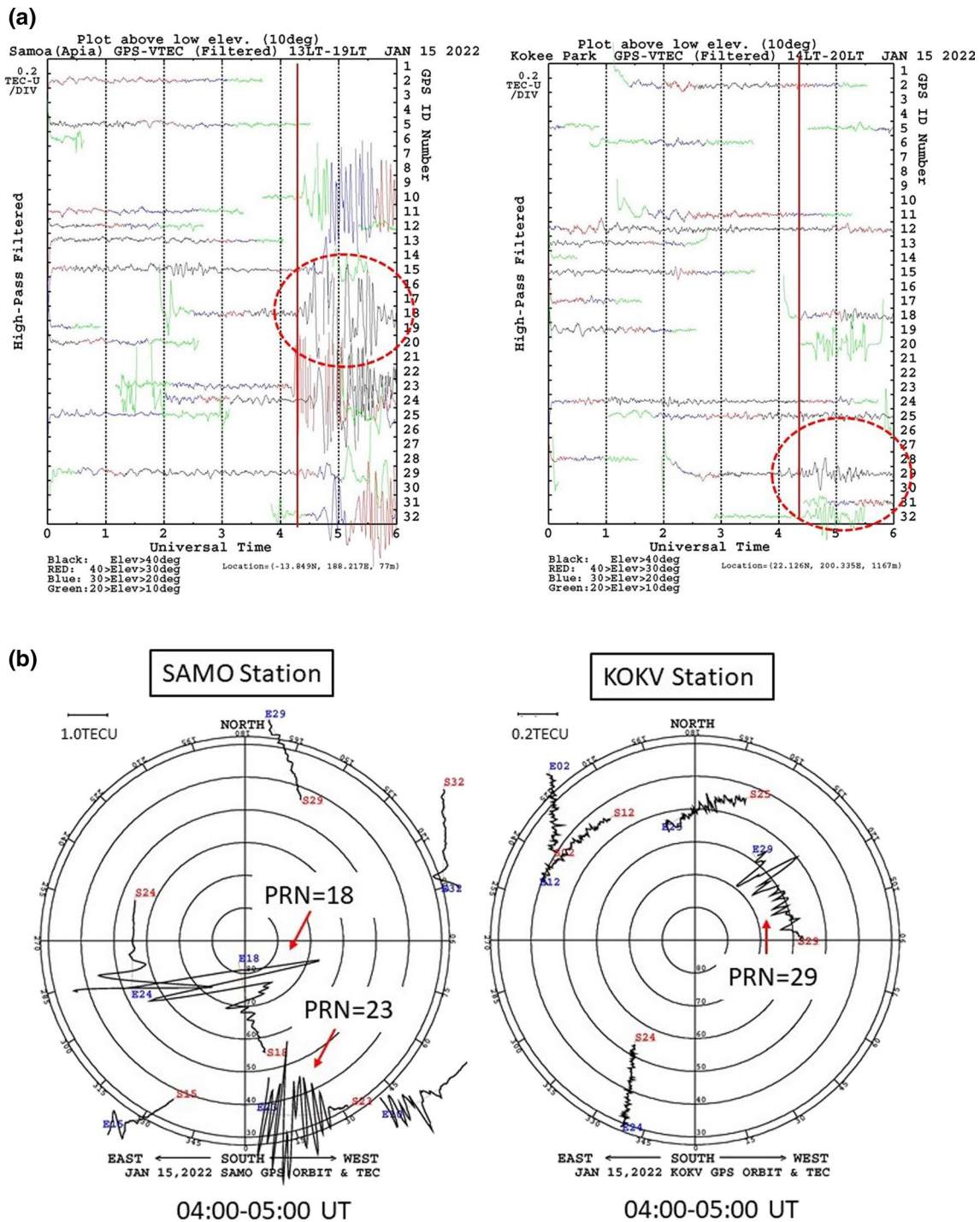
Figure 4a shows the GPS-TEC variation high-pass filtered with the same Gaussian-type filter applied to the geomagnetic data. The data at the SAMO station show a start of short-period oscillations around 04:15 UT (PRN23) just after the start of the volcanic eruption. At the KOKV station, a short-period oscillation seems to start at 04:20 UT (PRN29). Figure 4b shows the satellite directions of satellites seen from the receiver and the TEC variation in the sky viewed above from the ground. The azimuth angle is measured from the south to westward. The outer circle indicates the elevation angle = 30°. The time interval is from 04:00 to 05:00 UT. Only the data available throughout the time interval are plotted. Figure 4c shows the TEC variation and the satellite directions observed at the MKEA station similar to Fig. 4a and b.

Figure 5 shows enlarged plots of the TEC variation observed at the SAMO and KOKV to see the difference of timing and amplitude of oscillations for different GPS

satellites in more detail. The traces with very small amplitude are not shown. The difference in the timing probably comes from the difference in the IPP (Ionospheric Pierce Point) location which is the intersection of the line-of-sight (from a GPS receiver to a GPS satellite) with the ionosphere at an altitude 300 km.

Figure 6 shows, from top to bottom, the GPS-TEC variation at KOKV (PRN29), MKEA (PRN29), SAMO (PRN23) and at SAMO (PRN18). Although the amplitude at SAMO (PRN18) is more than 10 times larger than that of PRN29 observed at KOKV, a variation with similar shape, i.e., two peaks, appears with time-lag about 8.5 min. Note that the two-peak variation at KOKV (PRN29) leads that observed at SAMO (PRN18) by about 8.5 min. This time-lag is confirmed by a cross-correlation analysis shown later in this section. The amplitude of MKEA (PRN29) is much smaller than that of KOKV (PRN29) probably because the location of MKEA is more distant from the magnetic conjugate point of the volcano than that of KOKV.

Figures 7 and 8 show the MEM power spectral density (PSD) of geomagnetic variation and GPS-TEC variation for 04:30–05:30 UT (Fig. 7) and for 05:00–06:00



**Fig. 4 a** High-pass filtered GPS-TEC data observed at Samoa (SAMO, left panel) and Kokee Park, Hawaii (KOKV, right panel). At both stations, fluctuations start at around 04:15–04:20 UT about 1–6 min after the start of volcanic eruption. The different color of the lines indicates different elevation angle of the satellites as indicated under the panels. **b** The TEC variations along the directions of satellites seen from the receiver of the GPS satellites for KOKV (right panel) and for SAMO (left). The sky above the elevation angle = 30° viewed from the ground is shown. The azimuth angle is measured westward from the south. ‘Snn’ with red font indicates the start point (04:00 UT) of the PRN = nn satellite and ‘Enn’ with blue font indicates the end point (05:00 UT). Note that the scale is different for KOKV and SAMO, i.e., the unit scale shown at the upper left corner is 0.2 TEC unit (TECU) for KOKV and 1.0 for SAMO. **c** The TEC observed at the MKEA station. The format of each panel is the same as that in **a** and **b**

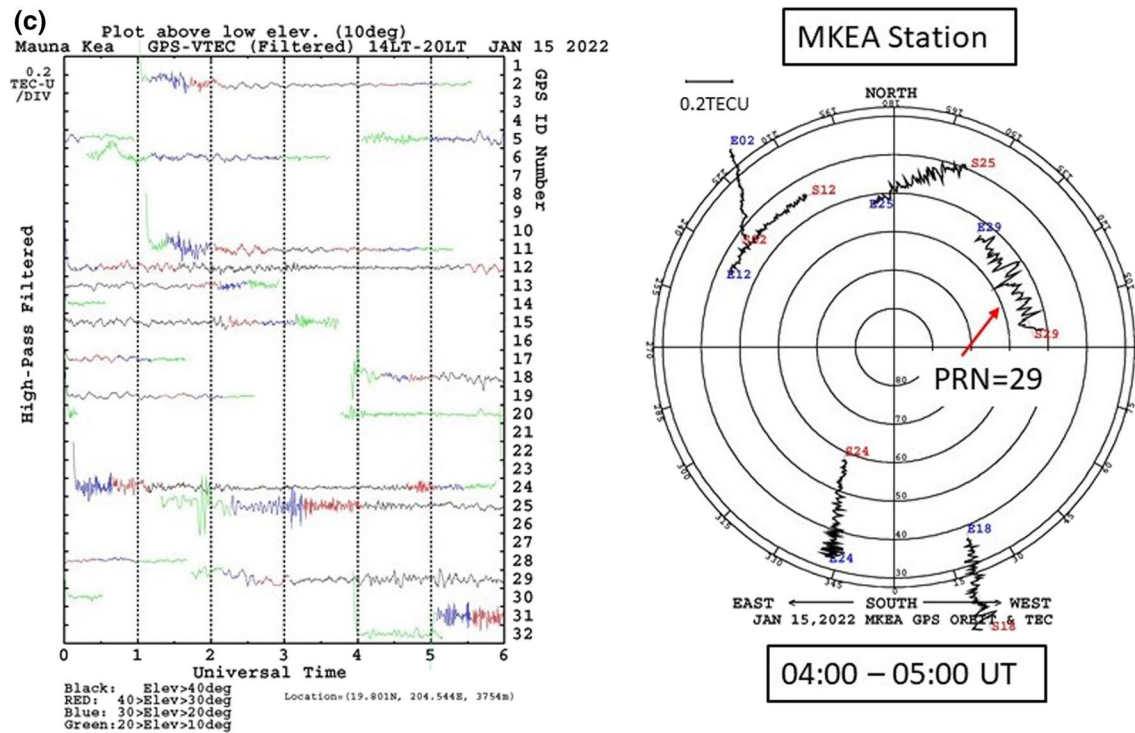
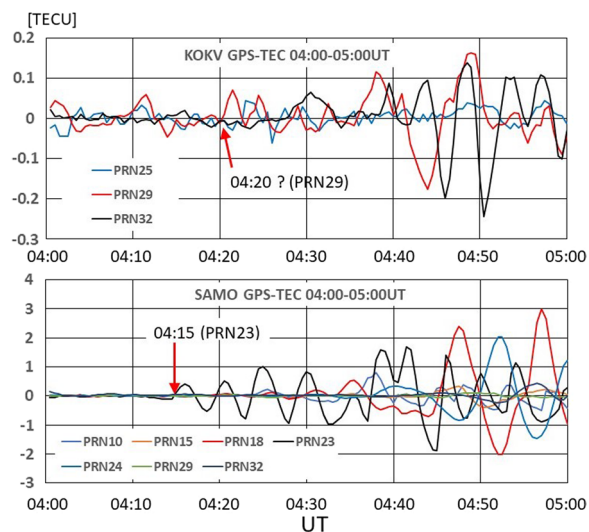
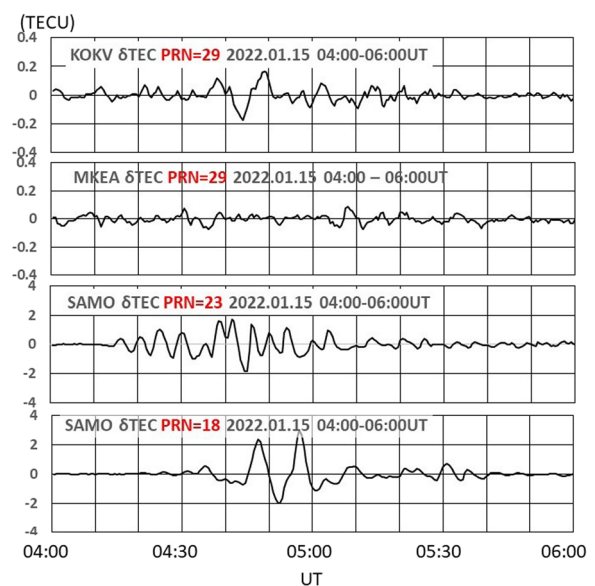


Fig. 4 continued



**Fig. 5** Enlarged plots of the TEC variations. The upper panel shows the high-pass filtered TEC data plots for 3 GPS satellites and the lower panel shows the plots for 7 GPS satellites. A wavy variation starts at 04:15 UT at SAMO and a similar but with much smaller amplitude variation start at 04:20 UT at KOKV station. Note that the scale for KOKV and SAMO is different



**Fig. 6** The GPS-TEC variation at, from top to bottom, Kokee Park, Kauai Is. (PRN29), Mauna Kea, Hawaii Is. (PRN 29), Samoa (PRN23) and Samoa (PRN18). Note that the scale is different between the upper two panels and the lower two panels. Although the amplitude at Samoa (PRN = 18) is more than 10 times larger than that of PRN = 29 observed at Kokee Park, a variation with similar shape, i.e., two peaks, appears with time-lag about 8.5 min. The TEC amplitude observed at MKEA is smaller than that observed at KOKV



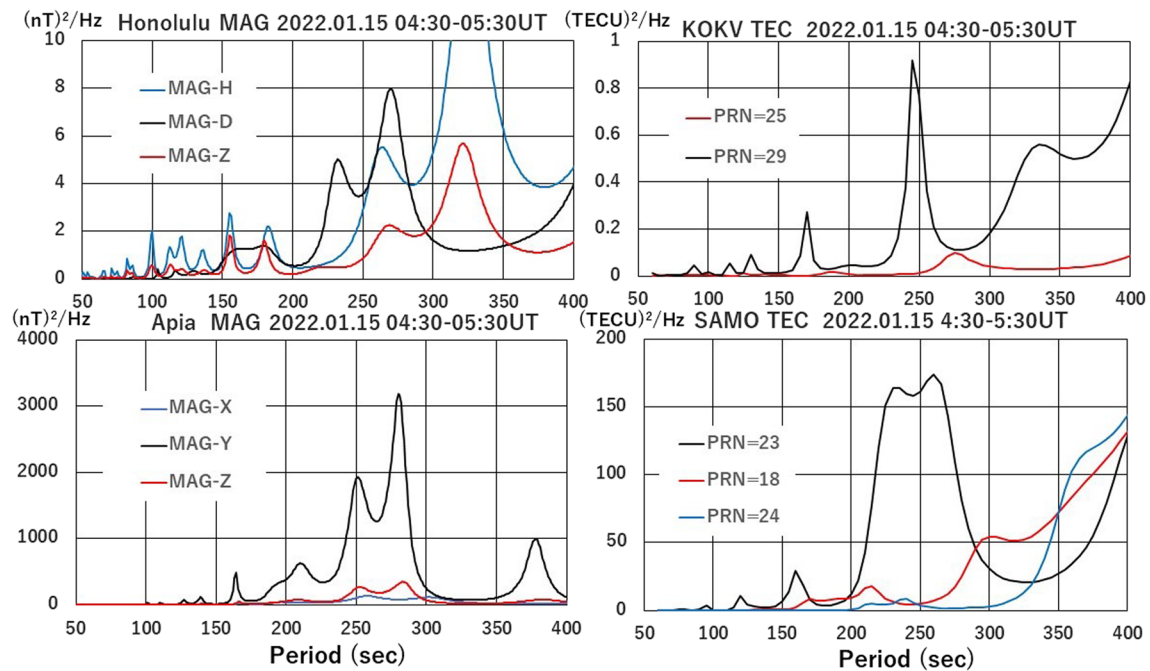


**Fig. 7** A comparison of power spectral density (PSD) of geomagnetic variation and GPS-TEC variation observed in Hawaii (upper panels) and those observed in Samoa (lower panels). The data from 04:30 to 05:30 UT were used to obtain the PSD by the MEM method with lag = 20 min

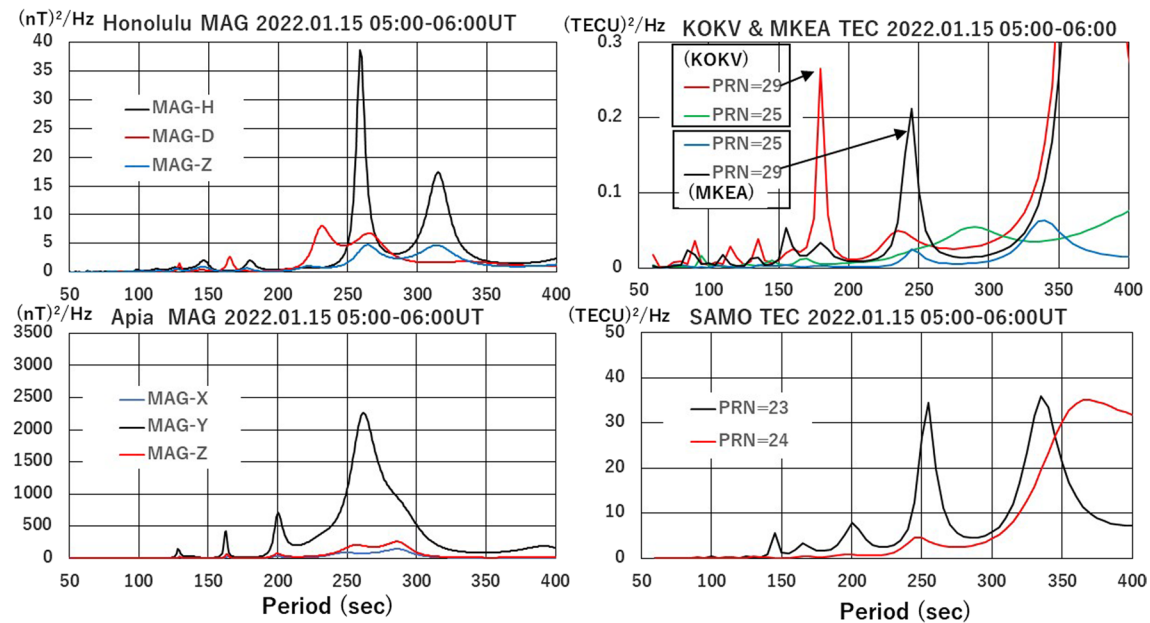


**Fig. 8** Same as Fig. 7, but with the data from 05:00 to 06:00 UT

UT (Fig. 8). The data length for PSD calculation used is one hour for the cases plotted in Figs. 7 and 8. Although the spectral peaks do not necessarily coincide exactly, the peaks roughly coincide between two geomagnetic

stations or among three GPS stations. In particular, the peaks at period 260 s for geomagnetic variation, or 250-s peaks for TEC variation commonly appear for 05:00–06:00 UT case. The period around 260 s is nearly



equal to the fundamental period of vertical acoustic resonance (e.g., Nishida et al. 2000; Shinagawa et al. 2007). A spectral peak around 250 s commonly appears in GPS-TEC data which is slightly different from the 260-s peak observed in geomagnetic data. It is not clear whether or not the peaks around 250 s are also the resonance peak but shifted by the Doppler effect caused by the movement of GPS satellite, or, shifted by some differences in the resonance condition, e.g., the atmospheric temperature profile or horizontal wind effect.

A clear peak at 180 s of KOKV (PRN29) in Fig. 8 (upper right panel) seems to correspond to the small peaks of MKEA (PRN29) and MAG-H at Honolulu in upper left panel. This period of 180 s is also close to second overtone (195 s) of the fundamental mode of the vertical acoustic resonance (e.g., Nishida et al. 2000; Shinagawa et al. 2007) and often appears in the TEC data under disturbed meteorological condition (e.g., Figs. 3, 7 or 19 in Iyemori et al. 2022). However, no appreciable peak at 180 s appears in SAMO data. Therefore, it could be a local phenomenon or the area of resonance of the second overtone was localized at the source area (i.e., near the volcano) and could not be detected at SAMO station. Note that the term "second overtone" used in this paper is not the same meaning with the term "second harmonic" normally used for the wave having the triple frequency of the fundamental frequency. In this paper, we use the term "second overtone" as the third resonance frequency caused by the height profile of the atmospheric density and temperature which determine the phase velocity of acoustic mode gravity waves. Three main resonance periods have been reported to exist at, for example, around 270 s (fundamental mode), 229 s (first overtone) and 196 s (second overtone) by Nishida et al. (2000), or 276 s, 228 s and 192 s, respectively, by Shinagawa et al. (2007) from their numerical simulation. These three resonance modes can be excited independently at a different location if a source disturbance exists there.

A cross-correlation analysis is applied to find the time-lag between the variations in the area near the volcanic eruption, i.e., in Samoa and in its geomagnetic conjugate area, i.e., in Hawaii. Figure 9 top panel (a) shows the normalized cross-correlation function of geomagnetic field oscillations in the east–west component between the data observed at Apia and those observed at Honolulu. The time-lag is very short, i.e., Apia leads only 23 s. The lower four panels, respectively, show, from the top, (b) the normalized cross-correlation between the TEC data at KOKV (PRN29) and those at SAMO (PRN18), (c) between KOKV (PRN29) and SAMO (PRN23), (d) between SAMO (PRN23) and SAMO (PRN18), and (e) between MKEA (PRN29) and SAMO (PRN23). The

data for a period from 04:00 to 06:00 UT are used. The peak time-lag,  $-13$  min, in panel (d) is consistent with the peak time-lags in panels (b) and (c), i.e., 4.5 min and 8.5 min, respectively, because  $4.5 + 8.5 = 13$  min.

The cross-correlation of geomagnetic oscillations clearly shows that the phase difference of the waves observed at Apia and Honolulu is exactly  $180^\circ$  with nearly zero time-lag in minute (but to be precise, Apia leads 23 s). This relation is also seen from enlarged plots in Fig. 10. A possible explanation of this anti-phase correlation is illustrated in Fig. 11. At a certain moment, the electric field generated in the ionospheric dynamo layer, i.e., in the E-layer, points eastward near the volcano and a field-aligned current flows as depicted in Fig. 11. Then a polarization electric field which accompanies a field-aligned current is transmitted to another hemisphere and points westward there. Because the magnetic effects from the field-aligned currents tend to be cancelled on the ground by the Pedersen currents in the ionosphere (Fukushima 1976), the magnetic effects we observe on the ground are considered to be generated mainly by the Hall currents. The Hall currents would flow in the direction depicted in the figure at the moment. If we observe its magnetic effect on the ground, we expect anti-phase relation because the Honolulu station is longitudinally distant from geomagnetic conjugate point of the volcano. That is, we observe the return current effect at Honolulu station.

The cross-correlation functions among the TEC variations presented in the four lower panels in Fig. 9 are not so simple as the case of geomagnetic variations. As expected from Fig. 6 top and bottom panels, the variations at KOKV (PRN29) start 8.5 min earlier than those at SAMO (PRN18). On the other hand, the variation at SAMO (PRN23) is 4.5 min earlier than that at KOKV (PRN29) and it is anti-correlation. The variations of SAMO (PRN23) and those of MKEA (PRN29) do not show any clear correlation peak [panel (e)]. The rapid decrease of the absolute value of the correlation coefficient toward both sides of the point with highest coefficient in the upper four panels suggests that the time-lag at the highest correlation coefficient is meaningful. On the other hand, the coefficients in the bottom panel do not have a clear peak and do not decrease toward both sides of lag-time axis, and this suggests no meaningful time-lag. Such variety in the cross-correlation functions for GPS-TEC data could come from the localized nature of TEC variation as seen in Fig. 4b and c.

To examine these results considering the location of TEC variations, the IPP at 300 km altitude is presented in Fig. 3 with yellow star marks. The IPP location at 04:30UT is (14.837 S, 188.200 E) for PRN18 and SAMO pair, (17.272 S, 187.065 E) for PRN23 and

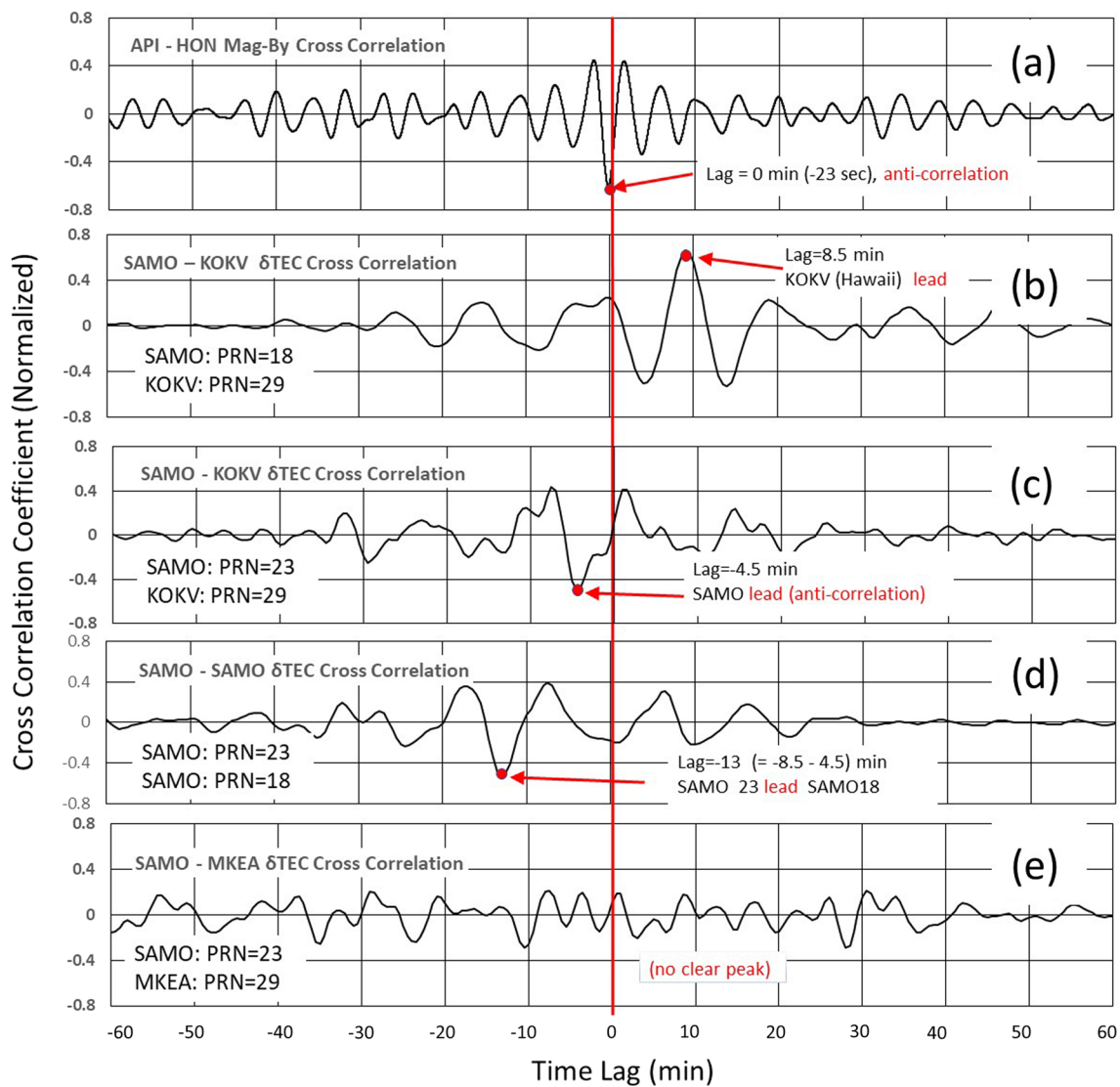


**Fig. 9** A cross-correlation function of geomagnetic oscillation between the data observed at Apia and Honolulu observatories (top panel **a**) and those of GPS-TEC variation between the data observed in Samoa and in Hawaii Islands (lower four panels) for a period from 04:00 to 06:00 UT. The highest correlation (absolute value) is marked by a red dot. No clear peak is seen for the case of the bottom panel **e**. The rapid decrease of the coefficient (absolute value) toward both sides of the point with highest coefficient in the upper four panels suggests that the time-lag is meaningful. On the other hand, the coefficients in the bottom panel do not have a clear peak and do not decrease toward both ends of time-lag axis

SAMO, (22.782 N, 199.002 E) for PRN29 and KOKV, and (20.656 N, 202.951 E) for PRN29 and MKEA. The earlier appearance of the variation with two peaks around 04:36 UT at KOKV (PRN29) than that around 04:45 UT at SAMO (PRN18) as seen in Figs. 5 or in 6 might come from the difference in the latitudinal difference from the volcano or its geomagnetic conjugate point. As presented by the yellow star marks in Fig. 3, the IPP of PRN29 for KOKV was rather close to the conjugate point in latitude than the latitudinal distance between the volcano and the

IPP of PRN18 for SAMO although the longitudinal distance is closer for PRN18 than the case for PRN29. On the other hand, the IPP of PRN23 for SAMO was most close to the volcano in the horizontal plane and this could cause the 4.5 min lead than the variation at KOKV (PRN29).

If the time-lags at the highest peaks of cross-correlation functions are meaningful, the results suggest that the  $\mathbf{E} \times \mathbf{B}$  drift (electric field drift) driven by the electric field transmitted to opposite hemisphere from volcanic

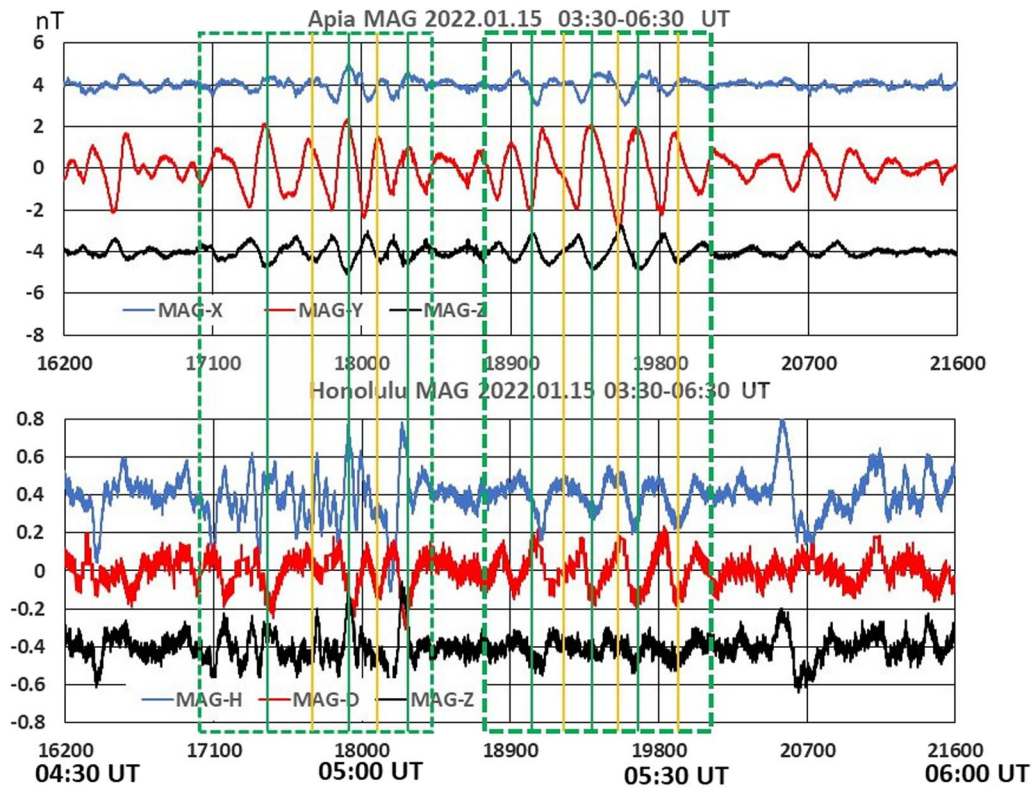


**Fig. 10** Phase relation of magnetic field oscillations between Apia and Honolulu

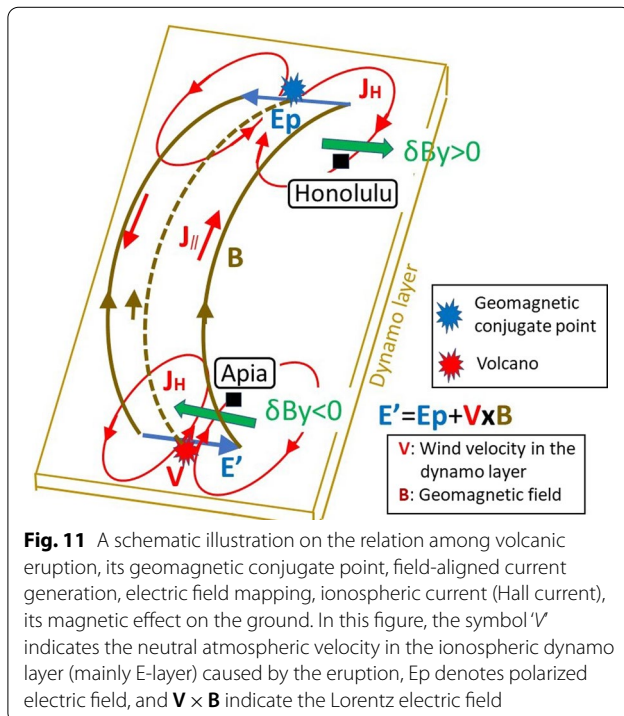


**Fig. 11** A schematic illustration on the relation among volcanic eruption, its geomagnetic conjugate point, field-aligned current generation, electric field mapping, ionospheric current (Hall current), its magnetic effect on the ground. In this figure, the symbol 'V' indicates the neutral atmospheric velocity in the ionospheric dynamo layer (mainly E-layer) caused by the eruption,  $E_p$  denotes polarized electric field, and  $V \times B$  indicate the Lorentz electric field

eruption area along the geomagnetic field is the most plausible cause of the TEC variation over Hawaii Islands. Here,  $E$  and  $B$  are the electric field and the geomagnetic field vectors, respectively, and eastward (westward) electric field causes upward (downward)  $E \times B$  plasma drift, resulting in the TEC variations. This is because the distance between Samoa (SAMO) and Hawaii (KOKV) is about 4192 km and it takes 17.5 min even with the speed of seismic S-wave, i.e., about 4 km/s, and this is too slow to explain the time-lag of 4.5 or 8.5 min. On the other hand, the Alfvén wave which transmit (accompany) the electric field takes only about 10–30 s or less to travel from Samoa to Hawaii.

Because the distance between the IPPs of PRN23 and PRN18 is about 296 km, if the time-lag of 13 min indicates the time necessary for a signal to propagate the distance, the velocity of a signal propagation is about 379 m/s which is roughly the acoustic wave velocity. This suggests that the time-lag of 13 min could be the time necessary for the acoustic wave propagation from IPP of PRN23 to the IPP of PRN18. That is, the time-lag of 8.5 min between KOKV PRN29 and SAMO PRN18 could be the time difference between the time necessary for an acoustic wave to propagate from the volcano to IPP (PRN18) and the time to the magnetic conjugate

point of the IPP between PRN29 and KOKV shown with a blue star symbol in Fig. 3 (left lower panel). The location of this conjugate point at 04:30UT was (19.8 S, 191 E), and the distance from the volcano was 673 km. The distance between the volcano and IPP (PRN23) and IPP (PRN18) were 445 km and 738 km, respectively. That is, the distance, 673 km, is in between 445 and 738 km, and hence, qualitatively consistent with an idea that the time-lags were caused by the necessary time for acoustic wave to propagate in the source region and the TEC variation in opposite hemisphere was caused by an electric field transmitted along geomagnetic field with very short ( $< 30$  s) time-lag.

The waveform of the magnetic oscillation around 05:10–05:40 UT (see Figs. 2 or 10) shows a sawtooth shape at both observatories. An example of geomagnetic variation observed during the 2004 Sumatra Earthquake, which is probably generated by a vertical acoustic resonance, also shows sawtooth waveform (Fig. 3 in Iyemori et al. 2005). Although we have no report on how commonly appear such sawtooth waveform at earthquakes or volcanic eruptions, we analyze

the waves observed in this Hunga Tonga event anticipating that the appearance of sawtooth waveform is a characteristic in such special events as earthquakes or sudden volcanic eruption and discuss a possible mechanism of the sawtooth wave generation.

In general, a sawtooth wave is formed by a combination of harmonic waves alternatively changing their sign. As shown in Fig. 12, if we calculate the PSD by FFT (Fast Fourier Transformation) for the sawtooth wave event, i.e., for 05:15–05:32 UT (1024 data points), we observe a harmonic structure of the fundamental mode of the vertical resonance, i.e., around 256 s in this plot, and its higher harmonics with periods 128, 85, 64, 51, and 43 s, etc. The sign (or the phase) of these harmonic waves changes alternatively as expected.

A MEM can give more precise period of the PSD peaks than an FFT method. That is, the fundamental frequency is 265 s which is the same with the theoretically expected fundamental resonance period and its higher harmonics detected by the MEM analysis are 136, 89, 67, 52, and 41 secs in this case. The appearance of the harmonic structure with alternatively changing sign of phase could be

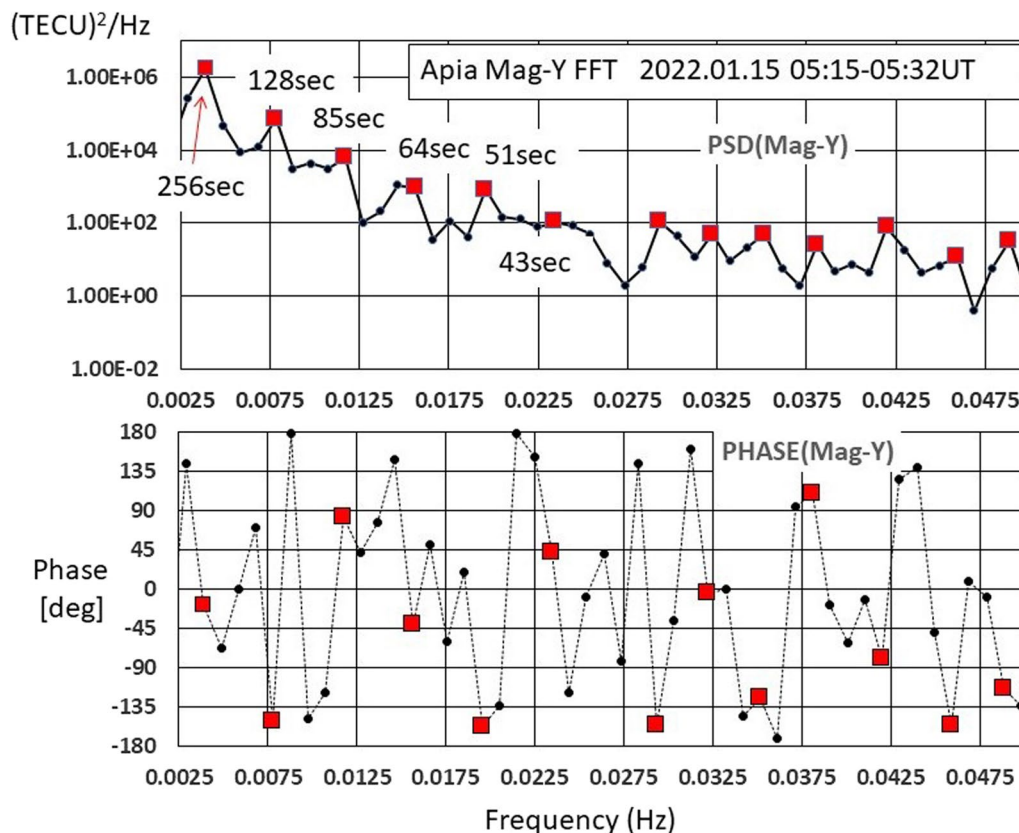


**Fig. 12** Harmonic structure of the PSD in 05:15–05:32 UT when a sawtooth waveform is observed (upper panel). Higher harmonics of the fundamental period around 265 s (256 s in this plot because of FFT algorithm) is seen. The lower panel shows the phase of each frequency component



a result of a complicated resonance process caused by a partial reflection in a vertical structure of acoustic wave cutoff periods. Or it could be a result of a rather simple process where the pressure on the ground starts to increase coherently in a wide frequency range of acoustic waves. The sudden volcanic eruption may satisfy this assumption. A vertical acoustic resonance could occur between the ground and the ionosphere at a fundamental frequency, i.e., one of the three main resonance frequencies (Nishida et al. 2000; Shinagawa et al. 2007), and also at its higher harmonics. A simple model calculation is presented in Appendix 1 to show a possibility of sawtooth waveform generation under such simple assumptions.

### Summary and conclusion

Just after the Tonga volcanic eruption, the geomagnetic oscillations observed with almost no time-lag (but to be precise, 23 s) at Apia and Honolulu located near the volcano and its geomagnetic conjugate point, respectively, indicated a period of vertical acoustic resonance. This confirms the formation of a field-aligned current system caused by an acoustic wave generated by the strong volcanic eruption. The GPS-TEC observations suggest the transmitted electric field along geomagnetic field from the opposite hemisphere to be the cause of the TEC variation observed in the geomagnetic conjugate area. That is, in some special cases, it is necessary to consider the effect of electric field transmission between the two hemispheres along geomagnetic field when we interpret a GPS-TEC variation.

The magnetic oscillations showed a sawtooth waveform. A possible generation mechanism of this sawtooth waveform observed both at Apia and Honolulu is presented. A simple mechanism presented in this paper (Appendix 1) suggests that the sawtooth waveform could be a characteristic in vertical acoustic resonance caused by a sudden pressure increase (or decrease) on the ground.

### Appendix 1

#### A simple model of sawtooth waveform generation

Following is an example of the situation where a sawtooth waveform of atmospheric pressure in the ionospheric dynamo layer is generated by a sudden increase of atmospheric pressure on the ground. This is a very simplified situation with assumptions and just to show a possible mechanism of sawtooth waveform generation.

Suppose that the fundamental frequency of vertical acoustic resonance wave to be  $\omega_1$  and wave number to be  $k_1$ .

If the resonance includes its higher harmonics, i.e.,  $\omega_2=2\omega_1$ ,  $\omega_3=3\omega_1$ , ...,  $\omega_n=n\omega_1$ , ..., and the higher harmonics also satisfy the resonance condition, then, the pressure variation,  $y$ , of the waves propagating upward and downward directions may be written respectively as;

$$y_{\text{up}} = a_1 \sin(k_1 x - \omega_1 t) + a_2 \sin(k_2 x - \omega_2 t) + a_3 \sin(k_3 x - \omega_3 t) + \dots \quad (1)$$

and,

$$y_{\text{down}} = a'_1 \sin(k_1 x + \omega_1 t) + a'_2 \sin(k_2 x + \omega_2 t) + a'_3 \sin(k_3 x + \omega_3 t) + \dots \quad (2)$$

and a superposition of these upward and downward propagating waves makes a resonance state.

Here,  $a_1, a_2, a_3, \dots, a_n, \dots$  and  $a'_1, a'_2, a'_3, \dots, a'_n, \dots$  are the amplitude of each component. The phase velocity is a constant, i.e., sound speed  $C_s = \omega_1/k_1$ , and the wave numbers are  $k_2=2k_1$ ,  $k_3=3k_1, \dots$ . We assume that the air pressure starts to increase at  $t=0$  for all higher harmonics on the ground and the acoustic wave propagate upward or downward with a sound speed  $C_s$ . That is, each harmonic component is also in a resonance.

The wave length of the fundamental wave,  $\lambda$ , is  $\lambda = 2\pi/k_1$ .

If  $a'_n = -a_n$

$$\begin{aligned} y = y_{\text{up}} + y_{\text{down}} &= \sum [a_n \{ \sin(k_n x - \omega_n t) - \sin(k_n x + \omega_n t) \}] \\ &= -2 \sum [a_n \cos(k_n x) \sin(\omega_n t)] \\ &= -2 \sum [a_n \cos(nk_1 x) \sin(n\omega_1 t)] \end{aligned} \quad (3)$$

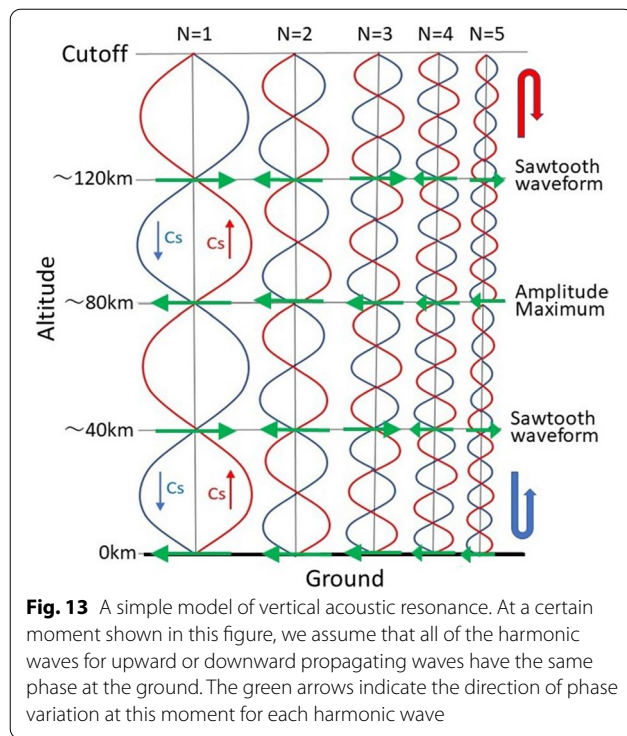
Here, the  $\Sigma$  means a summation for  $n=1, 2, 3, \dots$

At  $x = \lambda_1/2 = \pi/k_1$ ,

$$\begin{aligned} y &= -2 \sum [a_n \cos(n\pi) \sin(n\omega_1 t)] \\ &= -2 \left[ \sum \{ (-1)^n a_n \sin(n\omega_1 t) \} \right] \end{aligned} \quad (4)$$

That is, at a certain altitude, the phase of higher harmonics changes 180 degrees alternatively with  $n$ , and this can result a sawtooth waveform if the amplitude  $a_n$  ( $n=1, 2, 3, \dots$ ), have appropriate values. At the height  $x=3\lambda/2, 5\lambda/2, \dots, m\lambda/2$  ( $m$ : odd number)..., the situation is the same.

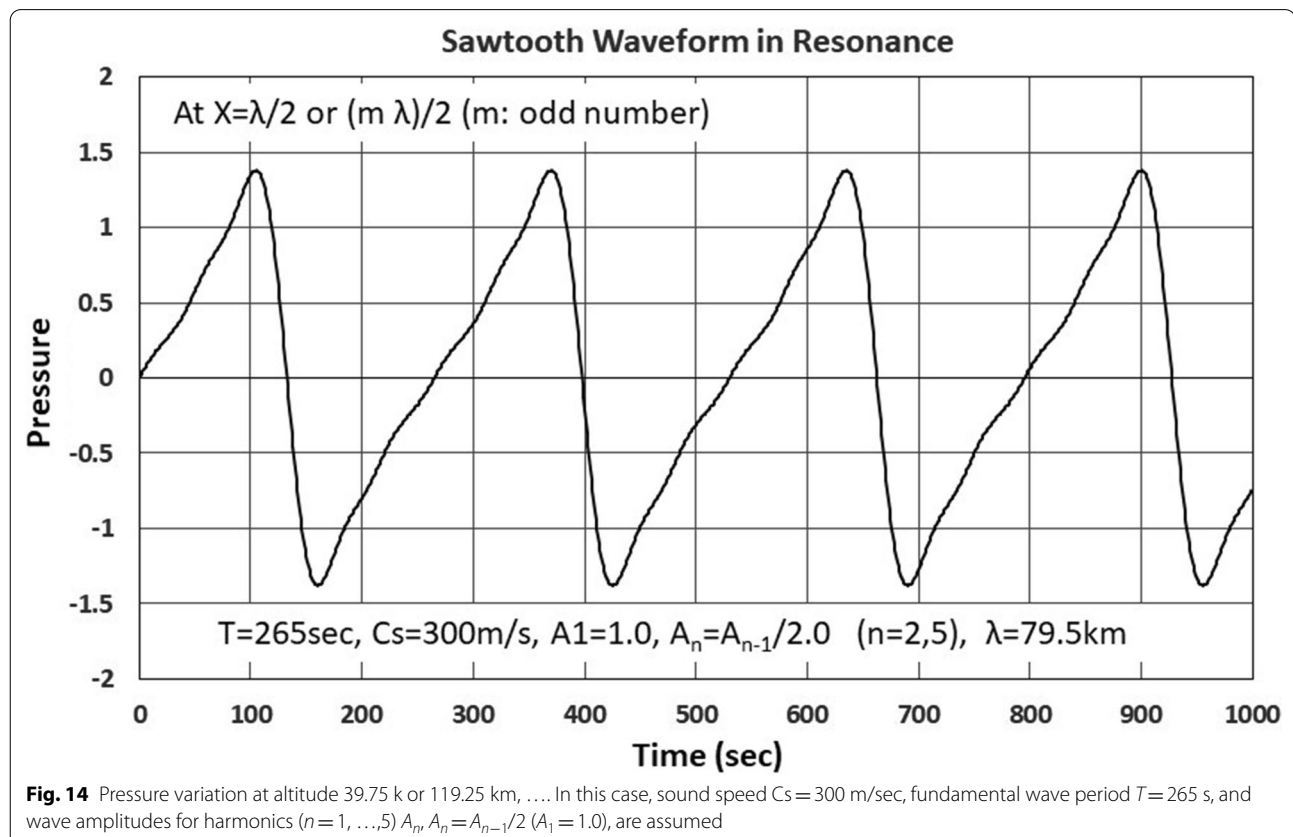
For the acoustic wave between the ground and around 120 km altitude, the average sound speed is  $\sim 300$  m/s.



For the wave with period 265 s, the wave length is 79.5 km.

Figure 13 shows the simplified situation we assume here. We assume that the waves are reflected at the ground and at the height where the sound waves encounter their cutoff, and stay in resonance for a while. At altitude around 40 km or 120 km, the direction of the phase variation indicated by green arrows changes the sign alternatively with the number of harmonics. That is, at these altitudes, a sawtooth waveform can be formed with appropriate amplitude combination of the harmonics.

Therefore, at 39.75 km, 119.25 km, ..., the waves show a sawtooth shape plotted in Fig. 14 if we assume the amplitude  $a_1 = 1$  and  $a_n = a_{n-1}/2$  ( $n=2, \dots, 5$ ). The essential points (assumptions) in this simple model are: (1) The pressure increase starts at the same time on the ground coherently for various harmonics (i.e., frequencies); and (2) higher harmonics also resonate in the same height range. It should be noted that the waveform at different altitude is not necessarily the sawtooth shape but various shapes are possible. It shows sawtooth at the specific height,  $m\lambda/2$  ( $m$ : odd number).



## Abbreviations

GPS: Global Positioning System; JSPS: Japan Society for the Promotion of Science; IGRF: International Geomagnetic Reference Field; IPP: Ionospheric pierce point; LT: Local time; MEM: Maximum entropy method; PSD: Power spectral density; TEC: Total electron content; TECU: TEC unit; UT: Universal time.

## Acknowledgements

The results presented in this paper rely on data collected at magnetic observatories. We thank the national institutes that support them and INTERMAGNET for promoting high standards of magnetic observatory practice ([www.intermagnet.org](http://www.intermagnet.org)). The GPS data and information on the GPS stations used in this paper are obtained from the web site of UNIVACO, Geoscience Australia, and SONEl (<https://www.sonei.org>). This study has been supported by the JSPS grants 15H05815, 17K05669, 20H00099 and 21K03643.

## Author contributions

TI conducted this research, collected the geomagnetic data, and mainly processed and analyzed the data. MN, YO and AS collected the GPS data and processed to derive the TEC values. TI, MN, YO and AS discussed the data and results of analysis. All authors read and approved the final manuscript.

## Funding

This study has been supported by the JSPS grants (Kakenhi) 15H05815, 17K05669, 20H00099 and 21K03643.

## Availability of data and materials

The one-second resolution geomagnetic data from Apia and Honolulu are downloadable from <https://intermagnet.org/data-donnee/download-eng.php>. The Receiver Independent Exchange (RINEX) format data used for GPS-TEC processing were provided by a non-profit university-governed consortium that facilitates geoscience research and education using Geodesy (UNAVCO) (<https://www.unavco.org/data/gps-gnss/gps-gnss.html>) for KOKV and MKEA and by the Geoscience Australia (<http://www.ga.gov.au/scientific-topics/positioning-navigation/geodesy/gnss-networks/data-and-site-logs>) for SAMO. The service of ionospheric conductivity calculation is available from a web page of the World Data Center for Geomagnetism, Kyoto (<https://wdc.kugi.yokyo-u.ac.jp/ionocond/sigcal/index.html>).

## Declarations

### Ethics approval and consent to participate

Not applicable.

### Consent for publication

Not applicable.

### Competing interests

The authors declare that they have no competing interests.

## Author details

<sup>1</sup>Graduate School of Science, Kyoto University, Kita-Shirakawa Oiwake-cho, Sakyo-ku, Kyoto 606-8502, Japan. <sup>2</sup>National Institute of Information and Communications Technology, Nukui Kita-machi, Koganei 184-8795, Japan. <sup>3</sup>Institute for Space-Earth Environmental Research, Nagoya University, Furo-cho, Chikusa-ku, Nagoya 464-8601, Japan.

Received: 16 February 2022 Accepted: 31 May 2022

Published online: 30 June 2022

## References

- Aoyama T, Iyemori T, Nakanishi K, Nishioka M, Rosales D, Veliz SEV (2016) Localized field-aligned currents and 4-min TEC and ground magnetic oscillations during the 2015 eruption of Chile's Calbuco volcano. *Earth Planets Space* 68(1):148. <https://doi.org/10.1186/s40623-016-0523-0>
- Calais E, Minster JB (1995) GPS detection of ionospheric perturbations following the January 17, 1994, Northridge earthquake. *Geophys Res Lett* 22:1045–1048. <https://doi.org/10.1029/95GL00168>

- Choosakul N, Saito A, Iyemori T, Hashizume M (2009) Excitation of 4-min periodic ionospheric variations following the great Sumatra-Andaman earthquake in 2004. *J Geophys Res* 114:A10313. <https://doi.org/10.1029/2008JA013915>
- Fukushima N (1976) Generalized theorem for no ground magnetic effect of vertical currents connected with Pedersen currents in the uniform-conductivity ionosphere. *Rep Ionos Space Res Japan* 30:35–40
- Iyemori T, Nosé M, Han D-S, Gao Y, Hashizume M, Choosakul N, Shinagawa H, Tanaka Y, Utsugi M, Saito A, McCreddie H, Odagi Y, Yang F (2005) Geomagnetic pulsations caused by the Sumatra earthquake on December 26, 2004. *Geophys Res Lett* 32:L20807. <https://doi.org/10.1029/2005GL024083>
- Iyemori T, Yamada A, Aoyama T, Hozumi K, Yokoyama Y, Odagi Y, Sano Y, Pang-sapa V, Jarupongsakul T, Saito A, Iguchi M (2022) Amplitude enhancement of short period GPS-TEC oscillations over rainfall area. *Earth Planets Space* 74:45. <https://doi.org/10.1186/s40623-022-01604-7>
- Kanamori H, Mori J (1992) Harmonic excitation of mantle Rayleigh waves by the 1991 eruption of Mount Pinatubo, Philippines. *Geophys Res Lett* 19:721–724. <https://doi.org/10.1029/92GL00258>
- Kanamori H, Mori J, Harkrider DG (1994) Excitation of atmospheric oscillations by volcanic eruptions. *J Geophys Res* 99:21947–21961. <https://doi.org/10.1029/94JB01475>
- Nishida K, Kobayashi N, Fukao Y (2000) Resonant oscillations between the solid Earth and the atmosphere. *Science* 287:2244–2246. <https://doi.org/10.1126/science.287.5461.2244>
- Nishioka M, Tsugawa T, Kubota M, Ishii M (2013) Concentric waves and short-period oscillations observed in the ionosphere after the 2013 Moore EF5 tornado. *Geophys Res Lett*. <https://doi.org/10.1002/2013GL057963>
- Otsuka Y, Ogawa T, Saito A, Tsugawa T, Fukao S, Miyazaki S (2002) A new technique for mapping of total electron content using GPS network in Japan. *Earth Planets Space* 54:63–70. <https://doi.org/10.1186/BF03352422>
- Saito A, Tsugawa T, Otsuka Y, Nishioka M, Iyemori T, Matsumura M, Saito S, Chen CH, Goi Y, Choosakul N (2011) Acoustic resonance and plasma depletion detected by GPS total electron content observation after the 2011 Tohoku Earthquake. *Earth Planets Space* 63:863–867. <https://doi.org/10.5047/eps.2011.06.034>
- Shinagawa H, Iyemori T, Saito S, Maruyama T (2007) A numerical simulation of ionospheric and atmospheric variations associated with the Sumatra earthquake on December 26, 2004. *Earth Planets Space* 59:1015–1026. <https://doi.org/10.1186/BF03352042>
- Zettergren MD, Snively JB (2015) Ionospheric response to infrasonic-acoustic waves generated by natural hazard events. *J Geophys Res Space Phys* 120:8002–8024. <https://doi.org/10.1002/2015JA021116>

## Publisher's Note

Springer Nature remains neutral with regard to jurisdictional claims in published maps and institutional affiliations.

**Submit your manuscript to a SpringerOpen<sup>®</sup> journal and benefit from:**

- Convenient online submission
- Rigorous peer review
- Open access: articles freely available online
- High visibility within the field
- Retaining the copyright to your article

Submit your next manuscript at ► [springeropen.com](https://www.springeropen.com)